Mathematical Medicine and Biology (2012) Page 1 of 24
doi:10.1093/imammb/dqs024

On the mechanics of a detaching retina

WILLIAM J. BOTTEGA* AND PETER L. BISHAY
Department of Mechanical & Aerospace Engineering, Rutgers University, Piscataway, NJ, USA
*Corresponding author: bottega@rci.rutgers.edu

AND

JONATHAN L. PRENNER AND HOWARD F. FINE
Retina Vitreous Center, Robert Wood Johnson University Hospital, UMDNJ, New Brunswick, NJ, USA

[Received on 13 October 2011; revised on 16 April 2012; accepted on 30 May 2012]

A mechanics-based mathematical model for retinal detachment is developed, incorporating an energy-based criterion for propagation. Retinas with and without central tears are considered and contraction of the vitreous and extension of its fibrils, along with a pressure difference across the retina, are taken as the stimuli for detachment propagation. In addition to the equations of motion, boundary and matching conditions, the variational formulation yields the self-consistent energy release rate that governs detachment, and formulae for critical stress and critical deflections that provide a rational basis for measuring critical parameters. Exact analytical solutions are established for axisymmetric detachment of retinas with and without tears, and numerical simulations are performed based on these solutions. The results yield characteristic behaviour, including threshold levels and stability of detachment, 'dimpling' of the detaching retina, the effects of changes in material and geometric parameters, and the influence of the presence and size of the retinal tear on detachment propagation. The model predicts that once detachment ensues it does so in an unstable manner and is extensive in scope. This is in agreement with clinical observation. Results also suggest that, under appropriate conditions, the presence and size of a retinal tear or hole can have a 'stabilizing' effect with regard to detachment propagation.

Keywords: retinal detachment; retinal tear; retina; vitreous contraction; vitreous fibril tension; subretinal pressure; spherical shell; elastic foundation.

1. Introduction

Retinal detachment is an affliction which affects many people and can lead to blindness. As a result of various causes, the multilayer retina can detach, typically along the interface between the retinal pigment epithelium (RPE), which is connected through Bruch's membrane to the outer part of the eye comprised of the choroid and the sclera on its outer surface, and the bulk of the retina—the nine layers of the sensory retina—on its inner surface. This usually occurs at the posterior of the eye, in the region of the posterior pole and the superior quadrants (see, for example, Wilkinson & Rice, 1997). According to Wilkinson & Rice (1997), the vitreous body is the most important intraocular tissue in pathogenesis of most types of retinal detachment. A detailed account of the anatomy of the retina and related parts of the eye, along with associated corrective surgery, is presented in that comprehensive text. According to Gariano & Kim (2004), who also discuss methods of treatment, the most common causes of retinal detachment are ageing, cataract surgery, myopia and trauma, and the most common type of retinal detachment is rhegmatogeneous (resulting from the accumulation of subretinal fluid).

Fine & Spaide (2009) presented intraoperative documentation of posterior precortical vitreous pockets (PPVP), a heretofore contested mechanism. The existence of PPVP has implications pertaining to mechanical effects and pathogenesis of posterior vitreous detachment, as well as of macular holes and shaken baby syndrome. While the issue of retinal detachment is certainly well known, the fundamental mechanics of detachment propagation has not, to this point, been adequately described. The purpose of the present study is to provide a substantial first step in elucidating the mechanics of the phenomenon.

From a mechanics perspective, retinal detachment involves dynamic processes acting over a very short time due to, say, jarring and impact, and involves very slow (quasi-static) processes occurring over many years. In one scenario for the latter, the vitreous tends to solidify and contract as we age, with the region near the retina becoming more fluid (Sebag, 1987). Concurrent to this, the (randomly dispersed) collagen fibrils of the vitreous develop interdigitation with the retina (cohesion on the macroscopic scale), thus exerting an inward pulling of the retina as the vitreous contracts. In addition, if a tear or hole develops or has developed in the retina, fluid can enter the gap (subretinal space) between the sensory retina and the RPE. The pressure exerted on the retina by the invasive fluid will generally counter the fluid pressure exerted on the vitreous side of the retina, in effect enhancing the pulling action of the vitreous fibrils. In the present study, we consider the effects of contraction of the vitreous and the action of its fibrils, as well as an induced interfacial pressure, as the stimuli for quasi-static retinal detachment propagation.

To our knowledge, no analytical studies directly pertaining to the mechanics of a detaching retina have been reported in the literature to date. However, several tests were conducted to measure certain mechanical properties of the retina, and mathematical models were proposed to assess mechanical characteristics of intact specimens. de Guillebon *et al.* (1971) and de Guillebon & Zauberman (1972) investigated the effect of peeling rate on the detachment behaviour, as well as the force required to detach the retina and the elongation of the retina in rabbit eyes. They observed that as the peeling rate increased, the detachment became unsteady and irregular, the force required for detachment increased logarithmically and the elongation became less pronounced. Wu *et al.* (1987) cut strips of retina aligned in two different directions relative to oriented blood vessels, subjected them to tension tests, and measured the associated load-deflection paths. They found that the orientation had minor effect on the overall results. They did, however, observe hysteresis under loading and unloading, and sensitivity to loading rate. Based on these results, they maintain that the retina is viscoelastic and the materials of the bond between the sensory retina and the RPE are also viscoelastic. Kain (1984) argued that the adhesion force between the sensory retina and the RPE is equal in all directions, on the basis of experimental measurements in which subretinal fluid was injected. Jones *et al.* (1992) measured Young's modulus of bovine retina. In their study, they bonded a circular specimen of retina to a relatively rigid annular disk. They then applied force to a string adhered to the centre of the unbonded region of the specimen, and measured the load-point deflection. Then, modelling the retina as a linear elastic isotropic membrane and assuming a Poisson's ratio of 0.49, they calculated Young's modulus of the retina from the data. In an analytical investigation, David *et al.* (1997) proposed to assess the reasons that myopic eyes tend towards retinal detachment by considering the application of the forces of the muscle in saccadic eye movements. Those authors considered a shell model of the eye subjected to a band loading of shear around the equator in the form of a temporal step function and predicted the corresponding dynamic axisymmetric response of the isotropic shell. They showed that the induced shear stress increases as the thickness of the eye wall decreases.

In related work, Hammer *et al.* (1986) measured the viscosity of subretinal fluid. Repetto *et al.* (2005) presented an idealized experimental study to simulate the motion of the vitreous humour due to saccadic eye movements. Among other things, they present the shear stress at the wall, as induced by

the simulated saccadic motion, and monitor its variation with viscosity. Many studies involving measurements of material properties of elements of the human eye, other than the retina, have been reported. However, as asserted by Asejczyk-Widlicka *et al.* (2011), the accurate determination of consistent material properties of eye components is difficult, and varying results are as numerous as the studies themselves due to differences arising from the techniques employed and the state of the tissue of interest prior to measurement. Eilaghi *et al.* (2010) conducted biaxial mechanical tests in the human sclera. Their test samples were taken in several locations of the globe of five donors and showed that the sclera is heterogeneous, near-isotropic and non-linear. Their measured value of the average low-strain biaxial modulus is comparable with the previously reported values of Woo *et al.* (1972a,b) whose method of testing was pressurization of the eye globe, and Friberg & Lace (1988) who employed uniaxial testing. Wollensak & Spoerl (2004) conducted a uniaxial test of the sclera and measured its modulus of elasticity for high strain. Asejczyk-Widlicka & Pierscionek (2008) measured the material properties of the sclera of porcine eyeballs. Their experiments showed that the material is isotropic and non-linear. In contrast, Bisplinghoff *et al.* (2009) measured the dynamic material properties using a high-rate pressurization system to create dynamic pressure. Their results showed that the stress–strain curves had a directional effect, thus demonstrating the anisotropy of the human sclera. Chen *et al.* (2009) and Chen & Weiland (2010), tested porcine eyes in air at room temperature, in saline at room temperature and in saline at body temperature. Their results showed that the properties of the retina are heterogeneous and anisotropic due to the size and orientation of the blood vessels in the retina, while the choroid and sclera were seen to be isotropic. They also studied the influence of temperature and surrounding material of the test samples on the stress–strain curves.

Most of the mathematical models of the human eye that have been developed to date focus on the outer coat of the eye (the sclera and cornea) in order to investigate the response of the globe to impact or to investigate globe rupture, while a few examine phenomena from certain medical procedures. Goldbaum *et al.* (1975) present a mathematical model for the effects of scleral buckles using a membrane model, while Michels *et al.* (1986) offer a discussion of the associated forces. Friberg (1989) presents a heuristic discussion of the causes and mechanisms of the formation of choroidal folds and implications with scleral buckle surgical techniques. Keeling *et al.* (2009) present a mathematical model of the mechanics of deformation of the eye due to an elastic band. They treat the eye as spherical, formulate the problem through a potential energy functional, arrive at analytical solutions and perform simulations. Voltairas *et al.* (2001) model retina reattachment by a magnetic tamponade. Most other studies are numerical in nature, involving Finite Element Models. Srodka & Iskander (2008) modelled the eye coat (sclera and cornea) using the finite element method (FEM) and modelled the eyeball as a spherical pressure vessel. The material properties they employed for the sclera were based on the measurements of porcine eyeballs by Asejczyk-Widlicka & Pierscionek (2008). The constitutive (stress–strain) relation assumed followed the empirical formula proposed by Nash *et al.* (1982) and Woo *et al.* (1972a,b). The material constants of this relation were found by matching the results of the finite element model with experimental measurements. Uchio *et al.* (1999) measured the elastic properties of the human cornea and sclera. They presented non-linear stress–strain curves from measurements made during uniaxial tension tests. They also determined Poisson's ratio to range between 0.455 (81-year-old male donor) and 0.48 (64-year-old female donor) with a mean value of 0.47. In addition, they developed a finite element model for the sclera and outer globe using shell elements, and for the vitreous gel using solid elements. Stitzel *et al.* (2002) developed a non-linear finite element model to predict the rupture of the globe as a result of trauma. They assumed that the materials were incompressible when considering Poisson's ratio, and used the same material properties for the cornea and sclera as Uchio *et al.* (1999) in their study. Hans *et al.* (2009) developed an FEM model to investigate the applied retinal forces

on the eyes of infants of age 6 months or younger during shaking, as the forces due to acceleration and deceleration of the eye may cause retinal haemorrhaging. The material properties they adopted for the various components of the eye were based on the data used in the models of Stitzel *et al.* (2002), Uchio *et al.* (1999), Graebel & van Alphen (1977), Jones *et al.* (1992) and Weber *et al.* (1982). The latter is related to Weber and Landwehr (1982). Replicating Jones *et al.* (1992), they assumed a Poisson's ratio of 0.49 (nearly incompressible material). Basinger *et al.* (2009) developed an FEM model of retinal prosthesis used to treat degenerative retina diseases by applying stimuli via an electrode array fixed to the retina. This study modelled the mechanical interaction between the eye wall (retina, choroid and sclera) and the electrode array (a solid device). The results were validated by qualitative comparison with surgical results. In their study, the authors used the elastic properties of the retina, choroid and sclera as measured by Chen *et al.* (2009).

As stated earlier, to our knowledge, no analytical studies directly pertaining to the mechanics of a detaching retina have appeared in the literature to date. In the present work, we present a mechanics-based mathematical model for retinal detachment, based on energy considerations. The problem is formulated as a propagating boundary value problem in the calculus of variations (see, for example, Bottega (1983)), and retinas with and without central tears are considered. Contraction of the vitreous and extension of its fibrils, along with a pressure difference across the retina, is taken as the stimuli for detachment propagation. By allowing the boundary of the detached region to vary, as well as that of a possible adjacent region of sliding contact, the variational formulation yields the self-consistent energy release rate that governs detachment, and formulae for critical stress and critical deflections that provide a rational basis for measuring critical parameters, in addition to the equations of motion, boundary and matching conditions. Exact analytical solutions are established for axisymmetric detachment of retinas with and without tears, and results are presented based on these solutions. The results reveal critical characteristic behaviour of the evolving ocular structure and the effects that various mechanical parameters have on this behaviour. We begin by formulating the mathematical problem.

2. Formulation

In this section we formulate the problem of quasi-static retinal detachment due to the action of fibrils that are extended from a contracted vitreous, as well as due to the presence of an intraocular pressure difference through the retina. In this first, idealized, model, we treat the eye, the retina, the sclera, and the choroid as spherical structures and consider axisymmetric deformations and detachment. In addition, all deforming structures are considered macroscopically isotropic.

Measured values of the thickness, h, and radius, R, of the retina[1] indicate that the thickness to radius ratio is typically $h/R \sim O(10^{-2})$. This suggests that a thin structure theory such as a shell theory is appropriate. Similarly, based on measurements of the (tangent) elastic modulus and thickness of the retina, the choroid and sclera that are available in the literature,[2] the ratio of the corresponding membrane stiffness of the retina, C, to that of the choroid C_{chor} and that of the sclera C_{scl} are found to be $10^{-4} < C/C_{\text{chor}} < 10^{-2}$ and $C/C_{\text{scl}} \sim O(10^{-3})$, respectively. The ratios of the bending stiffness of the retina, D, to the bending stiffness of the choroid, D_{chor}, and that of the retina to that of the sclera, D_{scl}, are found to be $10^{-6} < D/D_{\text{chor}} < 10^{-3}$ and $10^{-6} < D/D_{\text{scl}} < 10^{-4}$, respectively. In light of these factors, it is quite reasonable to model the retina as a thin elastic shell detaching from the interior of a rigid RPE–choroid–sclera composite structure. This is assumed in the following development.

[1] Wilkinson & Rice (1997), Asejczyk-Widlicka *et al.* (2011), Eilaghi *et al.* (2010), Woo *et al.* (1972b,a), Friberg & Lace (1988), Wollensak & Spoerl (2004), Asejczyk-Widlicka & Pierscionek (2008), Bisplinghoff *et al.* (2009) and Chen *et al.* (2009).
[2] Wilkinson & Rice (1997) and Chen *et al.* (2009).

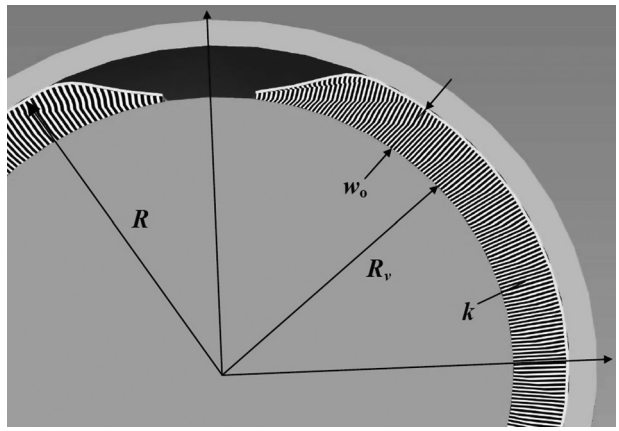

FIG. 1. Mathematical model of the eye, showing the contracted vitreous of radius R_v, the extended fibrils of stiffness k, the detached and intact segments of the retina (of radius R) with tear, and the RPE–choroid–sclera composite around the perimeter.

We shall consider the retina to be detaching axisymmetrically from a 'rigid' RPE–choroid–sclera foundation. In addition, the retina will be modelled as a spherical elastic shell of radius R, thickness h, Young's modulus E and Poisson's ratio ν. The membrane and bending stiffnesses of the retina are then $C = Eh/(1-\nu^2)$ and $D = Ch^2/12$, respectively (see, for example, Timoshenko & Woinowsky-Krieger, 1959). The vitreous gel and fibrils will be treated as a contracted elastic sphere, of which the radial stiffness density, k, is obtained in terms of the elastic modulus of the vitreous, E_v, its rest radius, R_v, and its Poisson's ratio, ν_v, if desired. Alternatively, the radial stiffness density, k, can be specified independently. With the retina modelled as a thin shell, the extended fibrils of a contracted vitreous then act as an effective, pre-tensioned, elastic 'foundation' of stiffness k per unit area with respect to the transverse deflection of the retina (Fig. 1). For simplicity, we shall assume symmetric deformation about the centre of the detached region. Spherical coordinates, (r, θ, φ), will be used to describe the evolving structure, where r is the radial coordinate, θ is the polar angle and φ is the azimuth angle. Symmetry is assumed about the $\varphi = 0$ axis and over the domain $0 \leqslant \theta \leqslant 2\pi$. In this context, the centre of the detached region will be located at the coordinates $r = R$, $\varphi = 0$. The domain of the retina is then $r \in [R - h/2, R + h/2]$, $\varphi \in [c, \pi]$, $\theta \in [0, 2\pi]$, where c is the meridian length (angle) of the tear. We shall consider both the case of a retina without a tear ($c = 0$) and the case of the retina with a tear ($c > 0$), as depicted in Fig. 2(a) and (b), respectively. The region of the retinal tear will be designated as S_0: $\varphi \in [0, c]$, while the detached segment of the retina will be divided into two regions; Region S_1: $\varphi \in [0, b]$, the 'lift zone', and Region S_2: $\varphi \in [b, a]$, the 'contact zone'. The latter corresponds to a region of sliding contact and borders on Region S_3: $\varphi \in [a, \pi]$, where the bond between the retina and the RPE remains intact.

The problem will be approached as a moving/propagating boundary value problem in the calculus of variations, where the interior boundary between the lift zone and contact zone, b, and the boundary between the contact zone and the intact region, a, are allowed to vary arbitrarily as well as the deflections of the retina along and transverse to the meridian. Towards this end, we first define a potential energy functional, Π, and introduce the transverse (radial) deflections, $w_j(\varphi)$ (positive inward) of the centre surface of the detached segment of the retina and its extension and the corresponding meridian deflections, $u_j(\varphi)$ (positive in the direction of increasing φ) within Region S_j ($j = 1, 2, 3$). The total

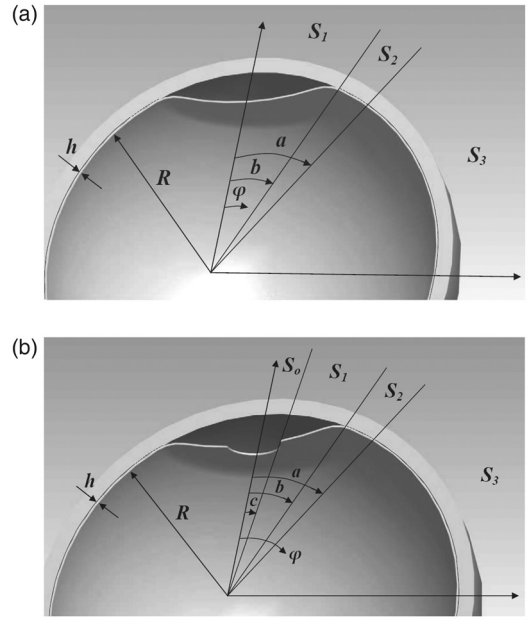

FIG. 2. Cross section of eye with detaching retina, depicting 'lift zone' S_1, 'contact zone' S_2 and 'intact region' S_3; (a) without retinal tear and (b) with retinal tear in region S_0.

potential energy, Π, of the ocular system modelled as described above is then

$$\Pi = U_{\mathrm{R}} + U_{\mathrm{v}} - \mathcal{W} - \Lambda + \Gamma \tag{2.1}$$

In the above functional, the elastic energy of the vitreous gel and fibrils, U_{v}, is given as

$$U_{\mathrm{v}} = 2\pi R^2 \sum_{j=1}^{3} \int_{S_j} \tfrac{1}{2} k (w_0 - w_j)^2 \sin\varphi \, \mathrm{d}\varphi \tag{2.2}$$

where w_0 corresponds to the (uniform) contraction of the vitreous surface (and hence the extension of the fibrils) and k is the corresponding radial stiffness per unit area of the vitreous fibrils.[3] The elastic strain energy of the retina, U_{R}, is comprised of bending energy and membrane (stretching) energy and, for the present formulation, takes the form

$$U_{\mathrm{R}} = 2\pi R^2 \sum_{j=1}^{3} \int_{S_j} [\tfrac{1}{2} M_{\varphi\varphi}^{(j)} \chi_{\varphi\varphi}^{(j)} + \tfrac{1}{2} M_{\theta\theta}^{(j)} \chi_{\theta\theta}^{(j)} + \tfrac{1}{2} N_{\varphi\varphi}^{(j)} \varepsilon_{\varphi\varphi}^{(j)} + \tfrac{1}{2} N_{\theta\theta}^{(j)} \varepsilon_{\theta\theta}^{(j)}] \sin\varphi \, \mathrm{d}\varphi \tag{2.3}$$

where the constitutive relations, strain-displacement relations and curvature-displacement relations are given in the Appendix. In the above expression, the functions $M_{\varphi\varphi}^{(j)}$ and $M_{\theta\theta}^{(j)}$ are the bending moments in region S_j $(j = 1 - 3)$ about the axis perpendicular to the normal indicated by the subscript and the

[3] The stiffness k can be considered a measurable material parameter on its own or may be expressed in terms of the material and geometric properties of the (contracted) 'vitreous/fibrils sphere' [see Eqs (2.26) and (2.29)].

functions $N^{(j)}_{\varphi\varphi}$ and $N^{(j)}_{\theta\theta}$ are the components of the internal membrane force per unit length in the direction indicated by the subscript. In addition, $\varepsilon^{(j)}_{\varphi\varphi}(\varphi)$ and $\varepsilon^{(j)}_{\theta\theta}(\varphi)$ are the (normal) strains along the indicated directions in region S_j ($j = 1 - 3$) and $\chi^{(j)}_{\varphi\varphi}(\varphi)$ and $\chi^{(j)}_{\theta\theta}(\varphi)$ are the corresponding curvature changes.

The work, $\mathcal{W}$, done by the ocular pressure difference, p, in deforming the detached segment of the retina is

$$\mathcal{W} = 2\pi R^2 \int_{S_1} p w_1(\varphi) \sin\varphi \, d\varphi \tag{2.4}$$

The energy of detachment, Γ, is given by

$$\Gamma = 2\pi R^2 \int_{S_1} 2\gamma \sin\varphi \, d\varphi = 2\pi R^2 [2\gamma(\cos c - \cos a)] \tag{2.5}$$

where γ is the energy required to produce a unit area of detachment, a property of the particular interface and retinal materials.

Finally, we introduce the constraint functional, Λ, as

$$\Lambda = 2\pi R^2 \int_{S_2} \sigma_2 w_2 \sin\varphi \, d\varphi + 2\pi R^2 \int_{S_3} [\sigma_3 w_3 + \tau u_3] \sin\varphi \, d\varphi \tag{2.6}$$

to insure continuity of the in-plane components and of the transverse components of the displacements in the intact region, and continuity of the transverse components of the displacements in the contact zone. The parameters $\sigma_2(\varphi)$, $\sigma_3(\varphi)$ and $\tau(\varphi)$ are Lagrange multipliers, and physically correspond to the radial normal stress in region S_2 and the radial normal stress and meridian shear stress in region S_3, respectively.

The Principle of Stationary Potential Energy may be stated, in the present context, as

$$\delta\Pi = 0 \tag{2.7}$$

Substituting the various functionals into the above, performing the indicated operations and allowing the boundaries at $\varphi = a$ and $\varphi = b$ to vary, as well as the radial and circumferential components of the displacements, results in the equilibrium equations in each region, the associated boundary conditions, and the transversality conditions that govern the locations of the propagating boundaries.

Equilibrium equations

The *equations of equilibrium* for the retina follow from the variational formulation as:

$$\frac{1}{R}\tilde{Q}^{(j)\prime}_{\varphi} - \frac{1}{R}(N^{(j)}_{\varphi\varphi} + N^{(j)}_{\theta\theta}) \sin\varphi + k w_j \sin\varphi = \sigma_j \sin\varphi \quad (\varphi \in S_j; j = 1 - 3) \tag{2.8}$$

$$\tilde{Q}^{(j)}_{\varphi} + (N^{(j)}_{\varphi\varphi} \sin\varphi)' - N^{(j)}_{\theta\theta} \cos\varphi = -\tau_j R \sin\varphi \quad (\varphi \in S_j; j = 1 - 3) \tag{2.9}$$

where $()' = d()/d\varphi$. In addition,

$$w_2(\varphi) = 0 \quad (\varphi \in S_2), \quad u_3(\varphi) = w_3(\varphi) = 0 \quad (\varphi \in S_3) \tag{2.10}$$

In (2.8) and (2.9),

$$\sigma_1 = \hat{\sigma} = p + k w_0, \quad \tau_1 = \tau_2 = 0, \quad \tau_3 = \tau \tag{2.11}$$

and

$$\tilde{Q}^{(j)} \equiv Q_{\varphi}^{(j)} \sin\varphi = \frac{1}{R}\{(M_{\varphi\varphi}^{(j)} \sin\varphi)' - M_{\theta\theta}^{(j)} \cos\varphi\} \quad (j = 1, 2, 3) \tag{2.12}$$

The quantity $Q_{\varphi}^{(j)}(\varphi)$ is the resultant transverse (meridian) shear force per unit length in region S_j.

Boundary conditions

The corresponding *boundary conditions* for the detached segment of retina are, similarly, found from the variational formulation. When *no retinal tear/hole* exists ($c = 0$), the conditions at the inner boundary are found to be

$$u_1(0) = 0, \quad w_1'(0) = 0, \quad \tilde{Q}^{(1)}(0) \equiv \frac{1}{R}[(M_{\varphi\varphi}^{(1)} \sin\varphi)' - M_{\theta\theta}^{(1)} \cos\varphi]_{\varphi=0} = 0 \tag{2.13}$$

Alternatively, when a *(symmetric) retinal tear/hole* is present ($c > 0$), the inner boundary is 'free', and the corresponding boundary conditions are found as

$$N_{\varphi\varphi}(c) = 0, \quad M_{\varphi\varphi}^{(1)}(c) \sin c = 0, \quad \tilde{Q}_{\varphi\varphi}^{(1)}(c) = 0 \tag{2.14}$$

The remaining boundary conditions depend on the presence or absence of a contact zone (Region S_2). *When a contact zone is present*, the boundary conditions at its inner boundary, $\varphi = b$, are

$$\begin{aligned} &u_1(b) = u_2(b), \quad N_{\varphi\varphi}^{(1)}(b) = N_{\varphi\varphi}^{(2)}(b), \\ &w_1(b) = w_2(b), \quad w_1'(b) = w_2'(b), \quad M_{\varphi\varphi}^{(1)} \sin\varphi|_{\varphi=b} = M_{\varphi\varphi}^{(2)} \sin\varphi|_{\varphi=b}, \quad Q_{\varphi}^{(1)}(b) = Q_{\varphi}^{(2)}(b) \end{aligned} \tag{2.15}$$

and those at its outer boundary, the edge of the detached area ($\varphi = a$), are

$$u_2(a) = u_3(a), \quad w_2(a) = w_3(a), \quad w_2'(a) = w_3'(a) \tag{2.16}$$

When a contact zone is absent ($b = a$), Region S_2 does not exist and region S_1 constitutes the entire detached area. For this case, the conditions at the edge of the detachment are

$$u_1(a) = u_3(a), \quad w_1(a) = w_3(a), \quad w_1'(a) = w_3'(a) \tag{2.17}$$

Transversality conditions

The boundaries of the detached area and of the contact zone are not fixed. Rather, they are found as part of the solution to the problem. Allowing these parameters to vary arbitrarily when performing the variations yields the *transversality conditions* that establish the locations of the propagating boundaries a and b that correspond to equilibrium configurations of the evolving ocular system. We consider two possibilities: (i) a contact zone is present and (ii) a contact zone is absent.

(i) *If a contact zone is present*, the condition that establishes the contact zone inner boundary, $\varphi = b$, is found to be a statement of the continuity of curvature at that point. After incorporation of $(2.10)_1$ and

TABLE 1 *Summary of boundary and transversality conditions and their application*

Condition type	Contact zone present	Contact zone absent
Boundary	No tear: (2.13)—or—w/tear: (2.14)	No tear: (2.13)—or—w/tear: (2.14)
Boundary	(2.15) and (2.16)	(2.17)
Transversality	(2.18), (2.19) and (2.20)	(2.21)

the pertinent boundary conditions, the transversality condition reduces to the form

$$w_1''(b) = 0 \tag{2.18}$$

to which we add the qualification

$$w_1''(b^-) > 0 \tag{2.19}$$

to rule out penetration.[4] In addition, the transversality condition that establishes the detachment boundary, $\varphi = a$, takes the form

$$\mathcal{G}\{a\} = \frac{C}{2R^2} u_1'^2 \Big|_{\varphi=a} = 2\gamma \tag{2.20}$$

where the function $\mathcal{G}\{a\}$ is identified as the *energy release rate* (energy released per unit increase of detachment angle) of the detaching ocular system.

(ii) If a contact zone is *absent* ($b = a$), (2.18) is superfluous and the transversality condition that establishes the detachment boundary, $\varphi = a$, is given by

$$\mathcal{G}\{a\} = \frac{1}{2R^2}\left[\frac{D}{R^2}(u_1' + w_1'')^2 + C u_1'^2\right]_{\varphi=a} = 2\gamma \tag{2.21}$$

Equations (2.20) and (2.21) suggest the following Griffith-type *criterion for detachment propagation (Griffith, 1920); If* $\mathcal{G}(a_0) \geqslant 0$ *for some initial value,* a_0*, of the detachment angle, a, propagation of the detachment will occur with 'a' increasing until the equality is satisfied. If* $\mathcal{G}(a_0) < 0$*, propagation will not occur.*

The boundary and transversality conditions for each situation are summarized in Table 1.

Equations (2.8)–(2.21) constitute the formal statement of the detachment problem. We note that we do not consider torsion about the axis of symmetry through the centre of the detached region and that, for deformations of this type on uniform spheres, the shear stress within the major surface will vanish. In this case, the membrane forces are equal and it follows from (A.1), (A.3), $(2.16)_1$, $(2.17)_1$ and $(2.10)_2$ that

$$u(\varphi) = 0 \quad (\varphi \in S_1 + S_2) \tag{2.22}$$

Incorporating (2.22) into (A.3) and (A.4) and substituting the resulting expressions into (2.8) renders the equation for transverse equilibrium of the retina in Region S_1 to the form

$$\sin\varphi\bar{w}'''' + 2\cos\varphi\bar{w}''' + g_2(\varphi)\bar{w}'' + g_1(\varphi)\bar{w}' + \bar{k}_{eff}\sin\varphi\bar{w} = \bar{\sigma}\sin\varphi \tag{2.23}$$

[4] In Eq. (2.19), the quantity b^- indicates a value of φ infinitesimally close to, but less than, b.

where

$$g_1(\varphi) = \cot\varphi \csc\varphi + (1-\nu)\cos\varphi, \quad g_2(\varphi) = -(\csc\varphi + \nu\sin\varphi) \tag{2.24}$$

$$\bar{w}(\varphi) \equiv w_1(\varphi)/R, \quad \bar{\sigma} \equiv \hat{\sigma}R^3/D \tag{2.25}$$

$$\bar{k}_{eff} \equiv 2(1+\nu)\bar{C} + \bar{k} = 2(1+\nu)\bar{C}[1+\eta] \tag{2.26}$$

$$\bar{k} = R^4 k/D, \quad \bar{C} = R^2 C/D = 12/\bar{h}^2, \quad \bar{h} = h/R \tag{2.27}$$

In addition,

$$\eta = \frac{1}{2(1+\nu)}\frac{\bar{k}}{\bar{C}} = \frac{(1-\nu)}{2(1-2\nu_v)}\frac{\bar{E}_v}{\bar{h}\bar{R}_v} \tag{2.28}$$

is the corresponding 'stiffness factor',[5] where

$$\bar{E}_v = E_v/E, \quad \bar{R}_v = R_v/R \tag{2.29}$$

It is seen that the effective radial stiffness consists of the superposition of the effective stiffness provided by the retina itself and the radial stiffness of the vitreous fibrils, as per (2.26). If the vitreous fibrils are much more compliant in the radial direction than the retina is along the meridian ($\eta \ll 1$), then it is seen that the stiffness of the vitreous fibrils enters the problem primarily through the pre-stress due to the vitreous contraction—i.e. through $\bar{\sigma}$ as per $(2.11)_1$. It is reasonable to consider the radial stiffness of the vitreous to be predominantly supplied by the fibrils. Finally, the effect of lateral contraction of the extended fibrils may be expected to be minor, rendering $\nu_v \approx 0$. Now, the mathematical forms of the equation governing transverse motion, (2.8) or the reduced form of (2.23), are akin to those for a spherical shell on an elastic foundation, with the spring stress kw exerting a compressive stress that opposes the inwardly deflecting detached segment of the retina and the stress kw_0 imparting an effective pressure which is combined with the intraocular pressure difference, p, as given by $(2.11)_1$. However, it is important to emphasize that the vitreous fibrils are always extended and therefore are always in tension, with the corresponding tensile stress exerted on the retina equal to $k(w_0 - w)$. The form of the governing equations is convenient and provides a useful analogue for solving the mathematical problem, provided this point is kept in mind.

With the restatement of the governing equation established, we next turn to the transversality conditions. It follows from (2.20) and (2.22) that, for the current linear model, no further detachment will occur if a contact zone is present. If no contact zone is present, then propagation is governed by (2.21) which, for the present model, reduces to the form

$$\bar{\mathcal{G}} = \frac{1}{2}\bar{w}'^2(a) = 2\bar{\gamma} \tag{2.30}$$

where

$$\bar{\gamma} = \gamma R^2/D \tag{2.31}$$

Equation (2.23) can be solved to yield the normalized radial displacement field. Since the differential equation is linear, we may anticipate that the solution will be proportional to $\bar{\sigma}$. Hence, the solution will

[5] The fibrils extended from the contracted vitreous are treated as a continuous distribution over the inner surface area of the retina. The contribution to the effective stiffness in terms of these parameters is here computed by treating the vitreous fibril bundle as stretched from a concentric vitreous sphere.

be of the general form

$$\bar{w}(\varphi) = \bar{\sigma}\ \bar{W}(\varphi) \tag{2.32}$$

where $\bar{W}(\varphi)$ is a non-dimensional function (the 'deflection profile') that satisfies the boundary and matching conditions. When substituted into (2.30), this then gives the critical effective applied stress in the form

$$\bar{\sigma}_{cr} = \sqrt{\frac{4\bar{\gamma}}{\bar{W}'^2(a)}} \tag{2.33}$$

The critical 'crown-point' deflection will then be

$$\bar{\Delta}_{cr} \equiv \bar{w}(0)|_{\bar{\sigma}=\bar{\sigma}_{cr}} = \bar{\sigma}_{cr}\bar{W}(0) = \bar{W}(0)\sqrt{\frac{4\bar{\gamma}}{\bar{W}'^2(a)}} \tag{2.34}$$

The critical deflection can be measured, and the critical bond energy (CBE), γ, then determined. Studies can then be performed to assess the variation of the CBE due to various clinical factors and their implications.

3. Solution

In this section, we present solutions for the case when a retinal tear is present as well as for the case when it is absent. Toward these ends, (2.23) is solved for uniform $\bar{\sigma}$ and yields the general form

$$\bar{w}(\varphi) = A_1\mathcal{P}_\alpha(\cos\varphi) + A_2\mathcal{P}_\beta(\cos\varphi) + A_3\mathcal{Q}_\alpha(\cos\varphi) + A_4\mathcal{Q}_\beta(\cos\varphi) + \frac{\bar{\sigma}}{\bar{k}_{\text{eff}}} \tag{3.1}$$

where $\mathcal{P}_\alpha$ and $\mathcal{Q}_\alpha$ are Legendre Functions of order α and of the first and second kind, respectively, $A_1 - A_4$ are constants of integration, and

$$\alpha = \frac{\sqrt{3-2\nu-i\bar{Z}}-1}{2}, \quad \beta = \frac{\sqrt{3-2\nu+i\bar{Z}}-1}{2} \tag{3.2}$$

where

$$Z = 2\sqrt{4\bar{k}_{\text{eff}} - (1-\nu)^2} \tag{3.3}$$

Case 1: *No Retinal Tear*

For the case when there is no retinal tear, the domain of definition of the detached segment of the retina is $\varphi \in [0, a]$ (see Fig. 2(a)). However, the function $\mathcal{Q}_\alpha(\cos\varphi)$ is singular at the origin. Since, on physical grounds, we require that the deflections be finite at the origin and throughout the domain of definition, we require that the constants A_3 and A_4 vanish. These conditions are then the 'boundary conditions' at $\varphi = 0$, and replace $(2.13)_{2,3}$. Imposing these conditions and $(2.16)_{2,3}$ with $(2.10)_1$ on (3.1)

yields the normalized deflection field as

$$\bar{w}(\varphi) = \bar{\sigma}\, \bar{W}(\varphi) = \frac{\bar{\sigma}}{\bar{k}_{eff}} \left[1 - \frac{\lambda(\varphi)}{\lambda(b)} \right] \tag{3.4}$$

where

$$\lambda(\varphi) = \mathcal{P}_\alpha(\cos\varphi) - \mathcal{H}(b)\mathcal{P}_\beta(\cos\varphi) \tag{3.5}$$

and

$$\mathcal{H}(b) = \frac{\alpha+1}{\beta+1} \left\{ \frac{\mathcal{P}_{\alpha+1}(\cos b) - \cos b\, \mathcal{P}_\alpha(\cos b)}{\mathcal{P}_{\beta+1}(\cos b) - \cos b\, \mathcal{P}_\beta(\cos b)} \right\} \tag{3.6}$$

Substitution of (3.4) into (2.30) gives the explicit form of the transversality condition, and hence the energy release rate, as

$$\begin{aligned} &\bar{\mathcal{G}}\{a\} = \frac{1}{2} \left(\frac{\bar{\sigma}}{\bar{k}_{\text{eff}}} \right)^2 \left[\frac{1}{\lambda(a) \sin^2 a} \{\alpha \mathcal{F}_\alpha(a) - \mathcal{H}(a)\beta \mathcal{F}_\beta(a)\} \right]^2 = 2\bar{\gamma} \quad (b = a) \\ &\bar{\mathcal{G}}\{a\} = 0 \quad (b < a) \end{aligned} \tag{3.7}$$

where

$$\mathcal{F}_\alpha(\varphi) = \{\alpha \cos^2\varphi - (1+\alpha)\}\mathcal{P}_\alpha(\cos\varphi) + \cos\varphi \mathcal{P}_{\alpha-1}(\cos\varphi) \tag{3.8}$$

The critical stress and critical 'crown-point' deflection for the case of no contact zone then follow from (3.4) and (3.7), giving

$$\bar{\sigma}_{\text{cr}} = \bar{K}_a \bar{\Delta}_{\text{cr}} \tag{3.9}$$

where

$$\bar{K}_a = \bar{k}_{\text{eff}} \lambda(a) / [\mathcal{H}(a) + \lambda(a) - 1] \tag{3.10}$$

$$\bar{\Delta}_{\text{cr}} / \sqrt{2\bar{\gamma}} = \sqrt{2} \sin^2(a) [\mathcal{H}(a) + \lambda(a) - 1] / [\alpha \mathcal{F}_\alpha(a) - \mathcal{H}(a)\beta \mathcal{F}_\beta(a)] \tag{3.11}$$

and

$$\bar{\Delta} \equiv \bar{w}(0) \tag{3.12}$$

With the analytical solution established, we next consider the issue of the existence of a contact zone. The location of the contact zone/lift zone boundary, $\varphi = b$, is established by the corresponding transversality condition, (2.18), together with the associated qualification, (2.19). Substituting the solution, (3.4), into (2.18) and carrying through the calculations reduces the condition for the location of the contact zone boundary to the equality

$$\mathcal{S}_\alpha(b) = \mathcal{S}_\beta(b) \tag{3.13}$$

where

$$\mathcal{S}_\alpha(b) = \frac{\alpha}{\alpha+1} \left[\frac{\cos b\, \mathcal{P}_{\alpha-1}(\cos b) - \{1 + \alpha \sin^2(b)\}\mathcal{P}_\alpha(\cos b)}{\mathcal{P}_{\alpha+1}(\cos b) - \cos b\, \mathcal{P}_\alpha(\cos b)} \right] \tag{3.14}$$

Equation (3.13) will be satisfied only if $\beta = \alpha$. It is seen from (3.2) that $\beta = \alpha$ when the parameter Z vanishes. Further, it is seen from (3.3) that this occurs only for the special ocular system where

$$\bar{k}_{\text{eff}} = \frac{(1-\nu)^2}{4} \tag{3.15}$$

So, generally, there is no contact zone. For the very special systems in which (3.15) holds, (3.13) will be satisfied for any and all values of b. This situation, total contact, corresponds to the trivial case. So, in general, there will be no contact zone for this special case as well.

We next present the solution for a detaching retina possessing a retinal tear.

Case 2: *Retinal Tear/Hole Present*

We next consider the situation where a retinal tear/hole of meridian length c exits at the centre of the detached region. For this case, the domain of definition of the detached segment of the retina is $\varphi \in [c, a]$ (see Fig. 2(b)). Imposition of the pertinent boundary conditions, (2.14) and (2.17), gives the constants of integration, $A_1 - A_4$, as

$$\begin{Bmatrix} A_1 \\ A_2 \\ A_3 \\ A_4 \end{Bmatrix} = \begin{bmatrix} \mathcal{P}_\alpha(\cos b) & \mathcal{P}_\beta(\cos b) & \mathcal{Q}_\alpha(\cos b) & \mathcal{Q}_\beta(\cos b) \\ X_\alpha^{(1)}(b) & X_\beta^{(1)}(b) & Y_\alpha^{(1)}(b) & Y_\beta^{(1)}(b) \\ X_\alpha^{(2)}(c) & X_\beta^{(2)}(c) & Y_\alpha^{(2)}(c) & Y_\beta^{(2)}(c) \\ X_\alpha^{(3)}(c) & X_\beta^{(3)}(c) & Y_\alpha^{(3)}(c) & Y_\beta^{(3)}(c) \end{bmatrix}^{-1} \begin{Bmatrix} -\bar{\sigma}/\bar{k}_{\text{eff}} \\ 0 \\ 0 \\ 0 \end{Bmatrix} \tag{3.16}$$

where

$$X_\alpha^{(1)}(\varphi) = (\alpha+1)[\mathcal{P}_{\alpha+1}(\cos\varphi) - \cos\varphi \mathcal{P}_\alpha(\cos\varphi)]/\sin\varphi \tag{3.17}$$

$$Y_\beta^{(1)}(\varphi) = (\beta+1)[\mathcal{Q}_{\beta+1}(\cos\varphi) - \cos\varphi \mathcal{Q}_\beta(\cos\varphi)]/\sin\varphi \tag{3.18}$$

$$X_\alpha^{(2)}(\varphi) = (\alpha+1)[\{(\alpha+1)\cos^2\varphi - \alpha\}\mathcal{P}_\alpha(\cos\varphi) - \cos\varphi \mathcal{P}_{\alpha+1}(\cos\varphi)]/\sin^2\varphi \tag{3.19}$$

$$Y_\beta^{(2)}(\varphi) = (\beta+1)[\{(\beta+1)\cos^2\varphi - \beta\}\mathcal{Q}_\beta(\cos\varphi) - \cos\varphi \mathcal{Q}_{\beta+1}(\cos\varphi)]/\sin^2\varphi \tag{3.20}$$

$$\begin{aligned} X_\alpha^{(3)}(\varphi)/(\alpha+1) = {} & \{1+\cos^2\varphi - \alpha(\alpha+1)\sin^2\varphi\}\mathcal{P}_{\alpha+1}(\cos\varphi)/\sin^3\varphi \\ & - \{1+\cos^2\varphi - \alpha(\alpha+2)\sin^2\varphi\}\cos\varphi\mathcal{P}_\alpha(\cos\varphi)/\sin^3\varphi \end{aligned} \tag{3.21}$$

$$\begin{aligned} Y_\beta^{(3)}(\varphi)/(\beta+1) = {} & \{1+\cos^2\varphi - \beta(\beta+1)\sin^2\varphi\}\mathcal{Q}_{\beta+1}(\cos\varphi)/\sin^3\varphi \\ & - \{1+\cos^2\varphi - \beta(\beta+2)\sin^2\varphi\}\cos\varphi\mathcal{Q}_\beta(\cos\varphi)/\sin^3\varphi \end{aligned} \tag{3.22}$$

The explicit (and lengthy) forms of the constants $A_1 - A_4$ are easily generated from (3.16), but are omitted for brevity. The solutions presented in this section are next employed to perform simulations of the evolving ocular system.

4. Results

In this section we present results of simulations based on the analytical solutions presented in Section 3. Studies are presented for the case of a pre-existing retinal tear as well as for the case when no tear is present. Except where indicated, it is assumed that $\eta \ll 1$. That is, the stiffness of the vitreous is neglected when compared with the effective transverse stiffness of the retina in computing $\bar{k}_{\text{eff}}$. Results are presented in terms of the rescaled stress

$$\tilde{\sigma} = \frac{\bar{\sigma}}{\sqrt{2\bar{\gamma}}} \tag{4.1}$$

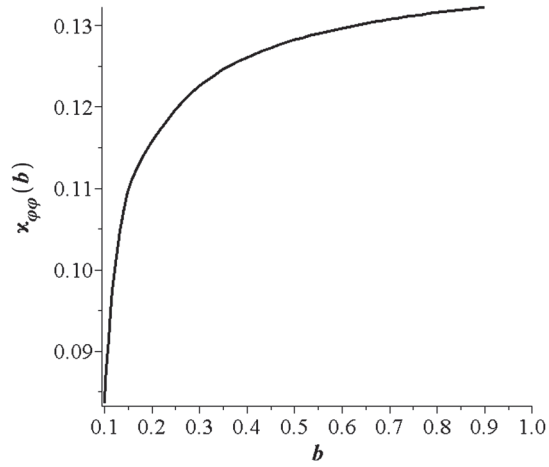

FIG. 3. The edge point curvature change per unit applied stress as function of lift zone size for retina with no tear; $\bar{h} = 0.008696$ and $\nu = 0.3$.

and rescaled 'crown-point' deflection

$$\tilde{\Delta} = \frac{\bar{\Delta}}{\sqrt{2\bar{\gamma}}} \tag{4.2}$$

Critical stresses and deflections are presented in the form of threshold paths and are generated using the solutions of the previous section together with the associated transversality condition established earlier. Each point on such a path corresponds to an equilibrium configuration of the evolving/detaching retina at the threshold level. Before proceeding, we first present a discussion of how to interpret the threshold paths presented. The criterion for detachment propagation following (2.21) states that propagation will not occur when the energy release rate is below the critical value, and hence when the effective stress is below its critical value. However, propagation will ensue when the energy release rate, and hence the associated critical stress, achieves its critical value and will continue until this ceases to be the case. Stability may be assessed by consideration of whether the critical stress (or deflection) in question indicated by the path increases or decreases monotonically with increasing detachment angle. For example, if the path is monotonically increasing, then an incremental increase in stress is required to produce an increment in detachment size. So, detachment propagation is stable in this case. If the path is, say, a U-shape (i.e. it initially decreases with detachment angle and then increases) then, when the stress achieves a critical value for a given detachment angle on the descending portion of the path, detachment will occur in an unstable manner at a constant stress level with detachment progressing dynamically until the upward segment of the path is reached. Subsequent propagation will be stable as an increment in stress is required to produce an increment in the detachment angle. If the threshold path is monotonically decreasing, then once the critical energy release, and hence the critical stress level, is achieved for a given detachment angle, it is achieved for all subsequent angles at that stress level. Therefore, for this case, detachment will be unstable and extensive (catastrophic).

We begin with a study of detachment for the case of no retinal tear.

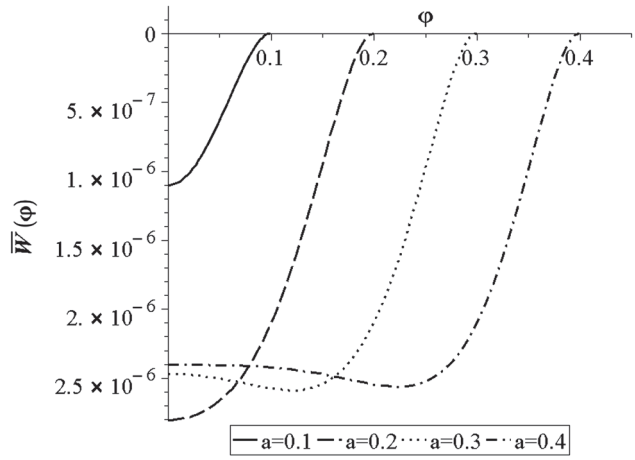

FIG. 4. Comparison of deflection profiles (per unit effective applied stress) for various detachment angles, for a retina with no tear, $\bar{h} = 0.008696$ and $\nu = 0.3$.

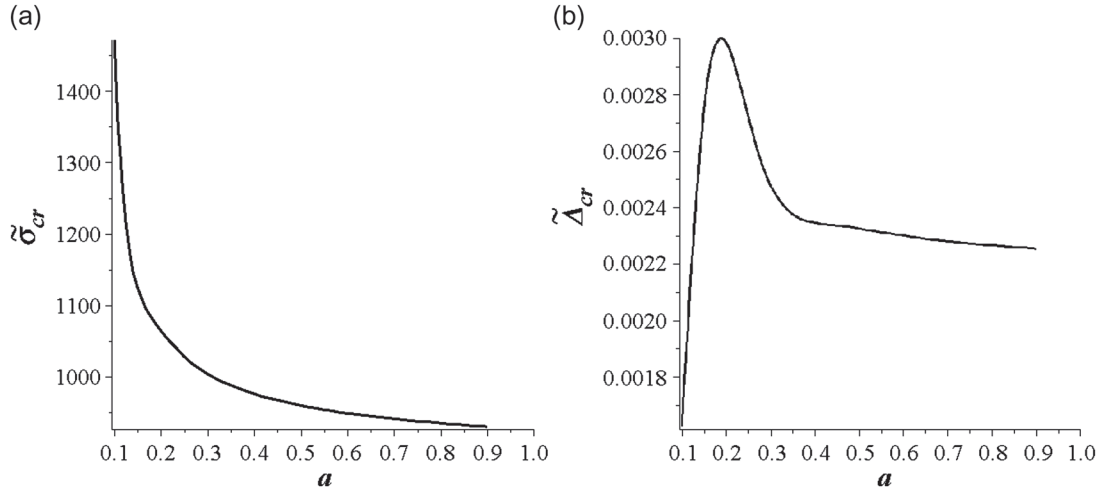

FIG. 5. Threshold paths for a retina with no tear, $\bar{h} = 0.008696$ and $\nu = 0.3$: (a) critical stress and (b) critical crown-point deflection.

4.1 *No Retinal Tear*

Results for a detaching retina without a retinal tear are presented in Figs 3–8. It was argued in Section 4 that a contact zone will not occur for this case. In support of this, we remark that no contact zone is observed for the range of detachment sizes considered[6] as verified by the plots of curvature change per unit applied stress presented in Fig. 3. As discussed in the previous section, and as seen from (3.4), the

[6] Contact zones were observed to occur for related studies of layered cylinders (Bottega, l988a–c,1994; Loia & Bottega, 1994; Bottega & Loia, 1996) for sufficiently large detachment angles. Such contact may be impeded, or prohibited, for spherical structures due to the added constraints imposed on the system and the effects of the associated stresses. The 'dimpling' observed for the spherical retina may occur in lieu of contact.

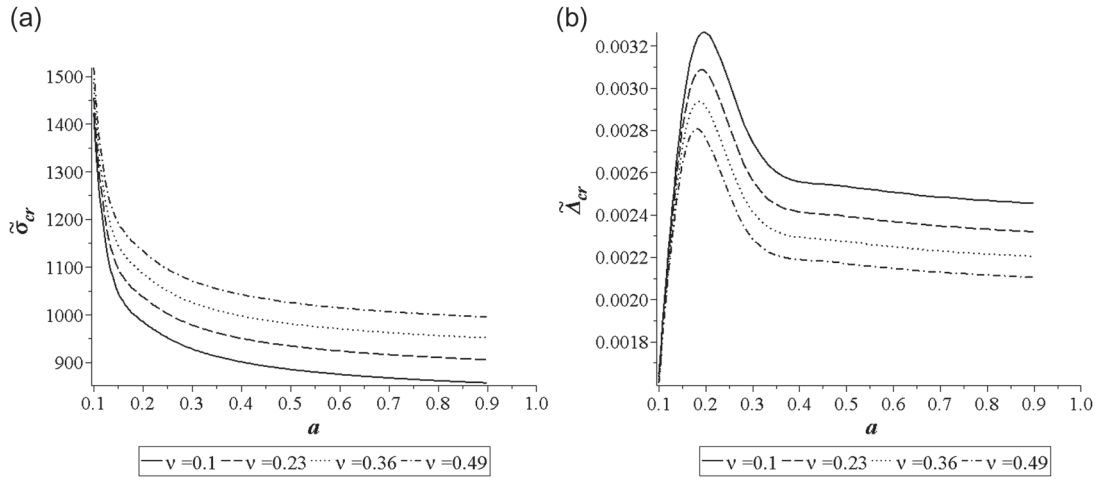

FIG. 6. Dependence of threshold paths on Poisson's ratio, for a retina with no tear, $\bar{h} = 0.008696$: (a) critical stress and (b) critical crown-point deflection.

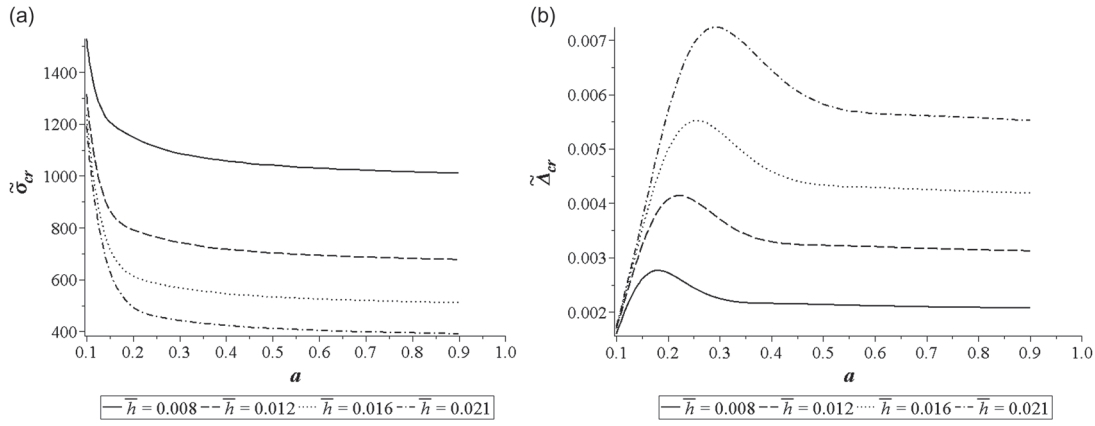

FIG. 7. Dependence of threshold paths on retina thickness to radius ratio, for a retina with no tear, $\nu = 0.3$: (a) critical stress and (b) critical crown-point deflection.

transverse deflection is directly proportional to the effective applied transverse stress, $\bar{\sigma}$. The deflection per unit transverse stress, $\bar{W}(\varphi)$, for various values of the detachment angle, a, is presented in Fig. 4 for the representative normalized thickness $\bar{h} = 0.008696$ and Poisson's ratio $\nu = 0.3$. It is seen that the deflection per unit stress increases as the size of the detached region increases. It is also seen that a 'dimple' develops when the area of the detachment is sufficiently large ($\varphi \geqslant 0.3$), and that the breadth and depth of the dimple increases accordingly. The critical stress for detachment propagation, $\tilde{\sigma}_{\mathrm{cr}}$, is presented in Fig. 5(a) as a function of detachment angle, a. It is observed from the figure that, for 'force controlled' loading (which is the case for a contracted vitreous with or without interfacial pressure), once detachment ensues it will continue in an unstable manner resulting in a very large area of detachment. This result is supported by clinical observations (see, for example, Wilkinson & Rice, 1997). The

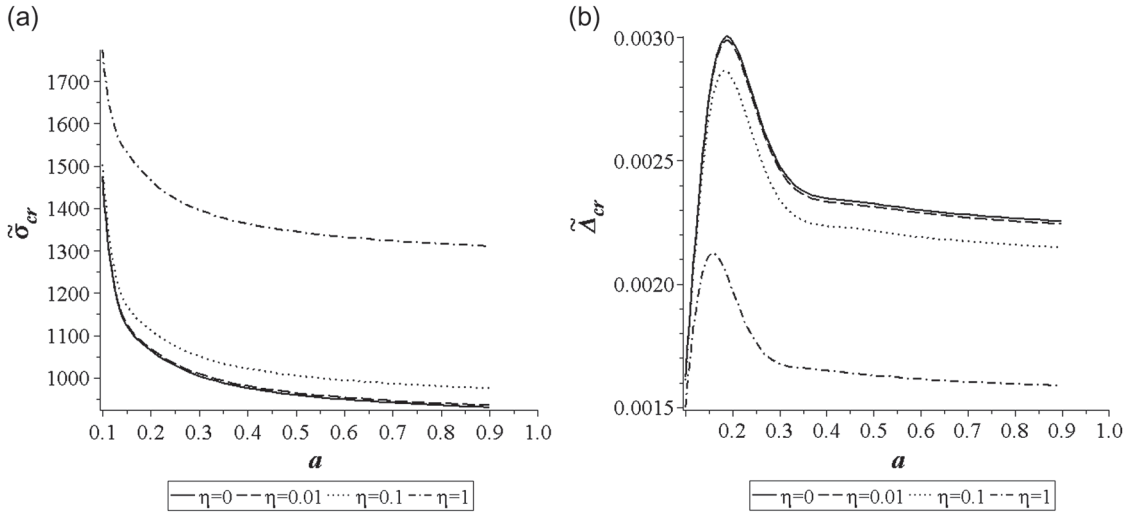

FIG. 8. Dependence of threshold paths on the vitreous/fibril stiffness parameter, for a retina with no tear, $\bar{h} = 0.008696$ and $\nu = 0.3$: (a) critical stress and (b) critical crown-point deflection.

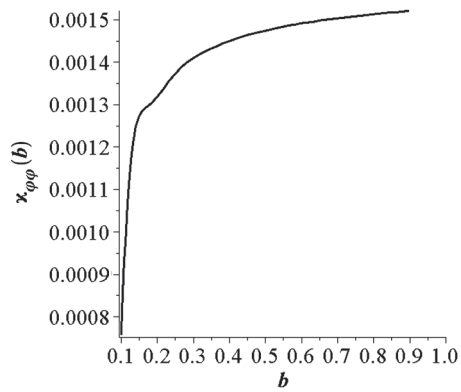

FIG. 9. Edge point curvature change per unit applied stress as function of lift zone size for torn retina; $\bar{h} = 0.008696$ and $\nu = 0.3$.

critical 'crown-point deflection', $\tilde{\Delta}_{\rm cr}$, is displayed in Fig. 5(b). The peak and subsequent monotonic decrease seen in the path are due to the presence of a dimple for larger values of the detachment angle. (That is, the crown-point deflection decreases though the overall deflection increases with a.) Therefore, this standard structural measure may be misleading for predicting and characterizing propagation for 'displacement-controlled' tests, but is useful for clinical measurements and can be used to determine the corresponding critical stress. The influence of Poisson's ratio and of the thickness to radius ratio of the retina on detachment is demonstrated by the threshold curves displayed in Figs 6 and 7, respectively.

Finally, the critical effective applied stresses and critical 'crown-point' deflections are presented for various values of the vitreous/fibril stiffness parameter, η, in Fig. 8(a) and (b). It is seen from these figures that, when the stiffness of the vitreous/fibrils is small compared with the effective radial stiffness of the retina, its influence on the characteristics of the behaviour of the system is negligible. If the

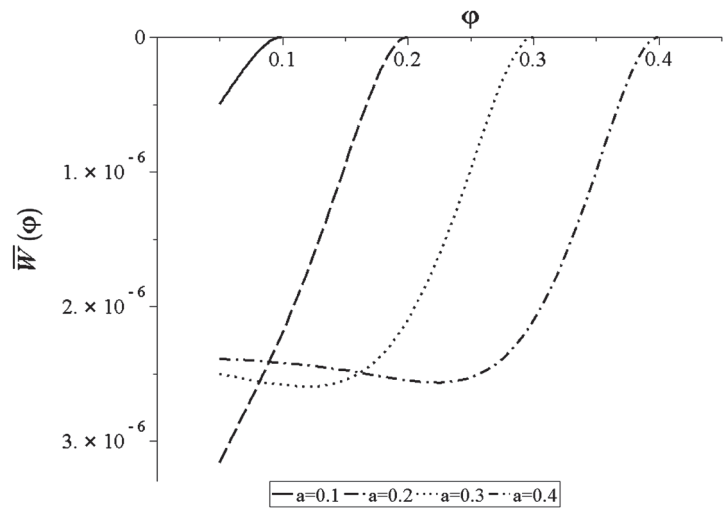

FIG. 10. Comparison of deflection profiles (per unit effective applied stress) for various detachment angles, for a torn retina with $c = 0.05$, $\bar{h} = 0.008696$ and $\nu = 0.3$.

vitreous/fibrils were to have appreciable stiffness, then the deflection (per unit effective applied stress) is reduced accordingly as $\eta \to O(1)$. It is observed from the critical stress paths of Fig. 8(a) that, if the vitreous/fibrils were to have appreciable stiffness, then the threshold stress for detachment is raised. One might wish to conclude from this that stiffening of the vitreous/fibrils could have an advantageous effect as far as detachment propagation is concerned. However, recall that increased k also implies increased effective applied stress, per (2.11). For a contracted vitreous, the fibrils are always extended and encourage detachment. The 'foundation effect', kw, is merely a reduction in the tension of the extended vitreous fibrils due to the inward deflection of the retina. In actuality, it is not a restoring force opposing the deflection. The corresponding critical 'crown-point' deflection paths are displayed in Fig. 8(b). We next examine the influence of a retinal tear on detachment propagation.

4.2 *Retinal Tear Present*

We next present corresponding results for retinal detachment for the case when a retinal tear of subtended angle c is present at the centre of the detached region (Figs 9–14). As for the case of no retinal tear, the deflections of the retina do not admit vanishing curvature at the edge of the lift zone, indicating that a contact zone is not possible. This is demonstrated in the plots of curvature change per unit applied stress for the representative case presented in Fig. 9. The deflection profiles per unit applied transverse stress are displayed in Fig. 10 for representative detachment angles, for a retina with a tear of angle $c = 0.05$ rad, thickness ratio $\bar{h} = 0.008696$ and Poisson's ratio $\nu = 0.3$. A dimpling effect similar to that seen for a retina without a tear is also observed. The corresponding critical stress and critical 'crown-point' deflection are displayed as a function of detachment angle in Figs 11(a) and (b). As for the retina without a tear, we see that once detachment ensues, it propagates in an unstable and catastrophic manner. However, the presence of the tear is seen to raise the threshold for propagation. This is due to the decrease in global stiffness (increase in flexibility) of the detached segment of the retina due to the presence of the tear, as well as the reduced resultant load over the surface and the corresponding reduction

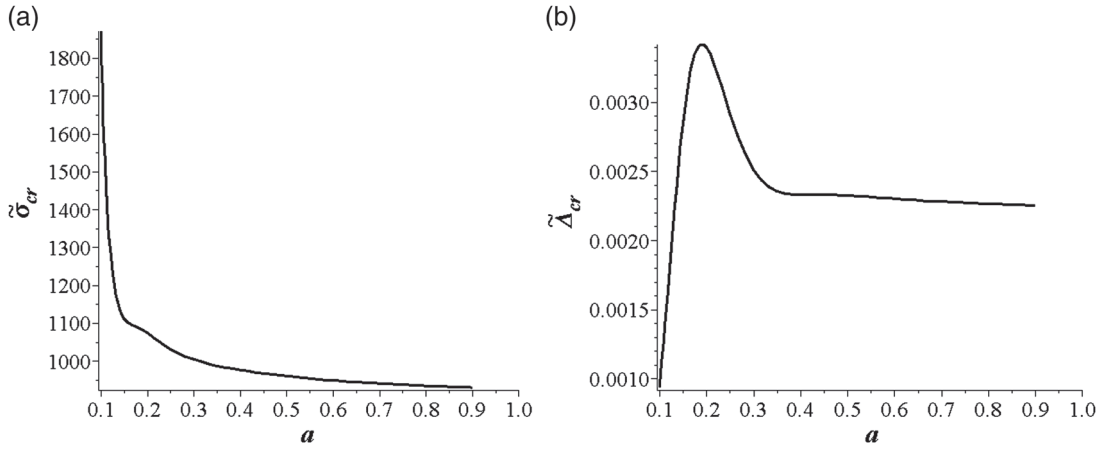

FIG. 11. Threshold paths for a torn retina with $c = 0.05$, $\bar{h} = 0.008696$ and $\nu = 0.3$: (a) critical stress and (b) critical crown-point deflection.

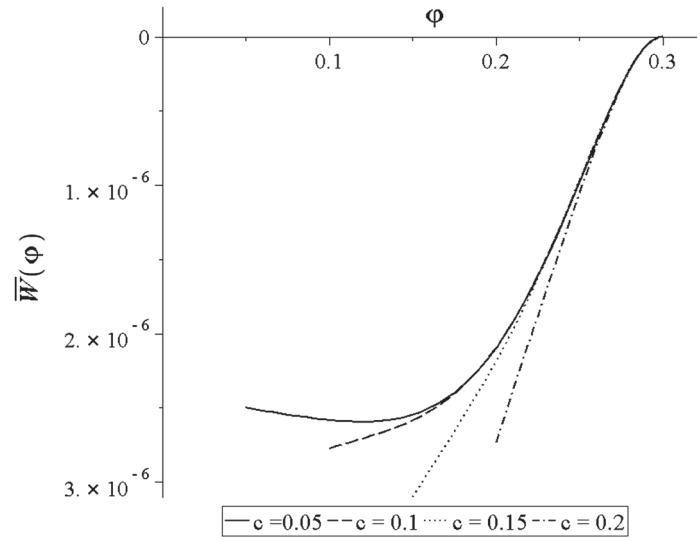

FIG. 12. Comparison of deflection profiles (per unit effective applied stress) for torn retinas with selected tear angles, $\bar{h} = 0.008696$ and $\nu = 0.3$.

of the associated moment about the detachment edge, a, imposed by the effective applied stress due to the diminished surface area of the detached segment of the retina.

We next examine the influence of the size of the retinal tear on detachment propagation through the results shown in Figs 12–14. The deflection profiles for several tear sizes are displayed in Fig. 12, for a detachment angle of $a = 0.3$ rad. It is seen that the larger the tear the larger the overall deflection for a given value of the effective applied stress. This can be attributed to the decreased global stiffness of the retina with increased tear angle c. A loss of dimple is also seen with increased tear size. Correspondingly,

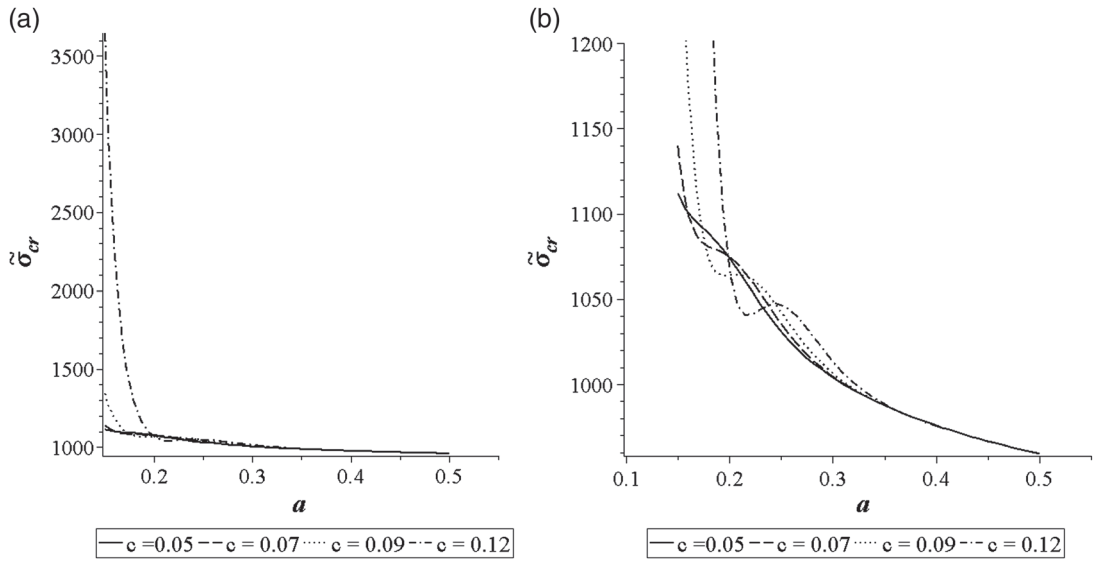

FIG. 13. Critical effective stress threshold paths for torn retinas with selected tear angles with $\bar{h} = 0.008696$ and $\nu = 0.3$: (a) 'large' stress range view and (b) 'local' stress range 'blow-up' view.

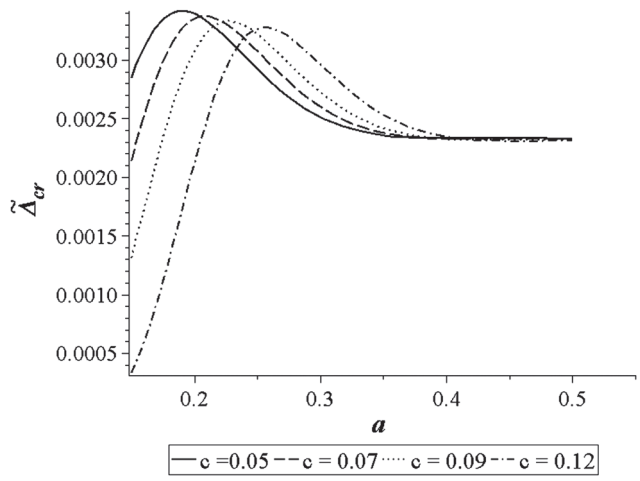

FIG. 14. Comparison of critical 'crown-point' deflection paths for torn retinas with selected tear angles, with $\bar{h} = 0.008696$ and $\nu = 0.3$.

it is seen from Fig. 13(a) that, at least for small detachment areas, the threshold stress increases with the size of the tear, but that all paths are asymptotic to one another as the detached area increases. Consideration of the enlarged view of portions of the paths (Fig. 13b) shows the presence of small, unstable, 'wells' that develop and increase in size with increased tear angle.[7] For the small range of

[7] These are reminiscent of the 'unstable wells' seen in the threshold paths for layered cylinders (see Bottega, 1988a–c,1994; Loia & Bottega, 1994; Bottega & Loia, 1996).

detachment angles within a 'well', small unstable but bounded growth of the detached area is possible for a limited range of the effective applied stress. The corresponding critical 'crown-point' deflections are displayed in Fig. 14.

5. Concluding remarks

A mechanics-based mathematical model for retinal detachment has been developed, as a propagating boundary value problem in the calculus of variations. The model assumes axisymmetric deformation and detachment, and treats the retina as an elastic shell while treating the much stiffer RPE–choroid–sclera composite structure as rigid. The vitreous and fibrils are modelled as a continuous spherical structure, whose effect is felt by the retina through the elastic stiffness of the extended fibril bundles. In this study, the stress resulting from contraction of the vitreous and the extension of its fibrils, along with pressure difference, are taken as the active drivers for detachment propagation. Retinas with and without central tears are considered. Linear strain-displacement relations are assumed for the retina, and the range of deflections and areas of detachment are suitably restricted. Propagation of retinal detachment is governed by a local energy criterion. Exact, closed form, analytical solutions of the axisymmetric boundary value problem for uniform effective stress (the sum of the pressure difference acting on the retina and the stress due to the vitreous contraction and full fibril extension) were obtained for a detaching retina with a tear as well as for a retina without a tear. A region of sliding contact of the retina with the RPE was assumed adjacent to the intact region. However, results indicated that no contact zone will be present.

Expressions for the critical effective stress for detachment propagation and for the corresponding critical retinal 'crown-point' deflection of the retina were established. These expressions can be used for experimental determination of the bond strength between the retina and the RPE and, due to their 3-D nature, will be more representative in assessing these quantities than a conventional 'peel test'. Results based on the analytical solutions revealed characteristic behaviour and the factors that contribute to that behaviour. We summarize the results below, for retinas without and with tears. We begin with retinas without a tear.

5.1 *Retinas with no tear*

It was seen that a contact zone between the lifted region and the intact region does not occur. However, it was observed that 'dimpling' of the detached segment of the retina does occur for 'larger' detachment angles, and that the size and depth of the dimple increase accordingly. As a result of the dimpling effect, measurements of bond strength based on displacement-controlled tests may be misleading or misinterpreted for all but very small detachment angles. However, the measured critical displacements can be used to determine the corresponding critical stress. Threshold paths for the applied effective stress indicate that detachment propagation is catastrophic for 'force-controlled' loading of the retina. That is, once propagation begins, it is extensive. This is in keeping with clinical observations.

Parameter studies were performed to examine the influence of various material and geometric properties of the retina on detachment propagation. Increasing the vitreous/fibril stiffness parameter is seen to raise the threshold level of the effective applied stress. However, raising the fibril stiffness also increases the applied effective stress by increasing the stress induced by the fully extended vitreous fibrils. Therefore, stiffening of the fibrils will not offer a panacea for impeding detachment propagation.

5.2 *Retinas with a tear*

It was demonstrated that, as for retinas without tears, no contact zone occurs between the lifted and intact regions of the detaching retinas considered. It was also seen that, as for retinas without tears, 'dimpling' of the detached segment of the retina occurs for large enough detachment sizes. The deflection of the detached segment of the retina per unit applied stress was observed to increase with increasing tear size. Detachment propagation was seen to be, generally, catastrophic. However, unlike for retinas without a tear, small regions of unstable 'wells' were observed in the threshold paths, and the depth and breadth of these wells were seen to increase with increasing tear size. Within these regions, unstable but finite detachment propagation is possible for a pre-existing detachment. Finally, the critical applied stress for detachment was seen to increase with tear size. This, together with the existence of unstable 'wells' in the threshold paths, leads one to conclude that tears have a stabilizing effect on detachment propagation. However, if a pressure jump across the detached segment of the retina exits as a result of the tear, and if it is substantial enough, then the applied stress may be higher in the presence of a retinal tear than without a tear for given vitreous contraction fibril stress, and the threshold levels more readily achieved. In contrast, if the pressure jump does not exist, or if it is negligible compared with the fibril tension, then the tear does appear to have a stabilizing effect with regard to detachment propagation.

References

Asejczyk-Widlicka, M. & Pierscionek, B. K. (2008) Elasticity and rigidity of the outer coats of the eye. *Br. J. Ophthalmol*. **92**, 1415–1418.

Asejczyk-Widlicka, M., Śródka, W., Schachar, R. A. & Pierścionek, B. K. (2011) Material properties of the cornea and sclera: a modelling approach to test experimental analysis. *J. Biomech.*, **44**, 543–546.

Basinger, B. C., Rowley, A. P., Chen, K., Humayun, M. S. & Weiland, J. D. (2009) Finite element modeling of retinal prosthesis mechanics. *J. Neural Eng.*, **6**, 1–9.

Bisplinghoff, J. A., McNally, C., Manoogian, S. J. & Duma, S. M. (2009) Dynamic material properties of the human sclera. *J. Biomech.*, **42**, 1493–1497.

Bottega, W. J. (1983) A growth law for arbitrary shaped delaminations in layered plates. *Int. J. Solids Struct.*, **19**, 1009–1017.

Bottega, W. J. (l988a) Peeling of a cylindrical layer. *Int. J. Fracture*, **38**, 3–14.

Bottega, W. J. (1988b) On thin film delamination growth in a contracting cylinder. *Int. J. Solids Struct.*, **24**, 13–26.

Bottega, W. J. (1988c) Debonding of a predeflected segment of a layer from the wall of a contracting cavity. *Eng. Fract. Mech.*, **31**, 1001–1008.

Bottega, W. J. (1994) On circumferential splitting of a laminated cylindrical shell. *Int. J. Solids Struct.*, **31**, 1891–1909.

Bottega, W. J. & Loia, M. A. (1996) Edge debonding in patched cylindrical panels. *Int. J. Solids Struct.*, **33**, 3755–3777.

Chen, K., Rowley, A. P. & Weiland, J. D. (2009) Elastic properties of porcine ocular posterior soft tissues. *J. Biomed. Mater. Res.*, **93A**, 634–645.

Chen, K. & Weiland, J. D. (2010) Anisotropic and inhomogeneous mechanical characteristics of the retina. *J. Biomech.*, **43**, 1417–1421.

David, T., Smye, S., James, T. & Dabbs, T. (1997) Time dependent stress and displacement of the eye wall tissue of the human eye. *Med. Eng. Phys.*, **19**, 131–139.

de Guillebon, H., de la Tribonniere, M. M. & Pomerantzeff, O. (1971) Adhesion between retina and pigment epithelium—measurement by peeling. *Arch. Ophthalmol.*, **86**, 679–684.

de Guillebon, H. & Zauberman, H. (1972) Experimental aspects of retinal peeling and stretching—biophysical aspects of retinal peeling and stretching. *Arch. Ophthalmol.*, **87**, 545–548.

Eilaghi, A., Flanagan, J. G., Tertunegg, I., Simmons, C. A., Brodland, G. W. & Ethier, C. R. (2010) Biaxial mechanical testing of human sclera. *J. Biomech.*, **43**, 1696–1701.

Fine, H. F. & Spaide, R. F. (2009) Visualization of the posterior precordial vitreous pocket in vivo with the triamcinolone. *Arch. Ophthalmol.*, **124**, 1663.

Friberg, T. R. (1989) The etiology of choroidal folds—a biomechanical explanation. *Graefes Arch. Clin. Exp. Ophthalmol.*, **227**, 459–464.

Friberg, T. R. & Lace, J. W. (1988) A comparison of the elastic properties of human choroid and sclera. *Exp. Eye Res.*, **3**, 429–436.

Gariano, R. F. & Kim, C.-H. (2004) Evaluation and management of suspected Retinal Detachment. *Am. Fam. Physician*, **69**, 1691–1698.

Goldbaum, M. H., Smithline, M., Poole, T.A. & Lincoff, H.A. (1975) Geometric analysis of radial buckling. *Am. J. Ophtalmol.*, **79**, 958–965.

Graebel, W. P. & van Alphen, G. W. (1977) The elasticity of sclera and choroid of the human eye, and its implications on scleral rigidity and accommodation. *ASME J. Biomech. Eng.*, **99**, 203–208.

Griffith, A. A. (1920). The phenomena of rupture and flow in solids. *Phil. Trans. R. Soc. London*, **22B**, 163–198.

Hammer, M. E., Burch, T. G. & Rinder, D. (1986) Viscosity of subretinal fluid and its clinical correlations. *Retina*, **6**, 234–238.

Hans, S. A., Bawab, S. Y. & Woodhouse, M. L. (2009) A finite element infant eye model to investigate retinal forces in shaken baby syndrome. *Graefes Arch. Clin. Exp. Ophthalmol.*, **247**, 561–571.

Jones, I. L., Warner, M. & Stevens, J. D. (1992) Mathematical modeling of the elastic properties of retina: a determination of Young's modulus. *Eye*, **6**(Pt 6), 556–559.

Kain, H. L. (1984) A new model for examining chorioretinal adhesion experimentally. *Arch. Ophthalmol.*, **102**, 608–611.

Keeling, S. L., Propst, G., Stadler, G. & Wackernagel, W. (2009) A mathematical model of the deformation of the eyeball by an elastic band. *Math. Med. Biol.*, **26**, 165–185.

Loia, M. A. & Bottega, W. J. (1994) Blister growth in layered cylinders. *Compos. Eng.*, **4**, 1275–1287.

Michels, R. G., Thompson, J. T., Rice, T. A. & Freund, D. (1986) Effect of sclera buckling on vector forces caused by epiretinal membranes. *Am. J. Ophthalmol.*, **102**, 44–451.

Nash, I. S., Greene, P. R. & Foster, S. C. (1982) Comparison of mechanical properties of keratoconus and normal corneas. *Exp. Eye Res.*, **35**, 413–424.

Repetto, R., Stochino, A. & Cafferata, C. (2005) Experimental investigation of vitreous humour motion within a human eye model. *Phys. Med. Biol.*, **50**, 4729–4743.

Sebag, J. (1987) Age related changes in human vitreous structure. *Graefes Arch. Clin. Exp. Ophthalmol.*, **225**, 89–93.

Srodka, W. & Iskander, R. (2008) An optically inspired biomechanical model of the human eyeball. *J. Biomed. Opt.*, **13**, 1–8.

Stitzel, J. D., Duma, S. M., Cormier, J. M. & Herring, I. P. (2002). A nonlinear finite element model of the eye with experimental validation for the prediction of globe rupture. *Stapp Car Crash J.*, **46**, 81–102.

Timoshenko, S. & Woinowsky-Krieger, S. (1959) *Theory of Plates and Shells*. New York: McGraw-Hill.

Uchio, E., Ohno, S., Kudoh, J., Aoki, K. & Kisielewicz, L. T. (1999) Simulation model of an eyeball based on finite element analysis on a supercomputer. *Br. J. Ophthalmol.*, **83**, 1106–1111.

Voltairas, P. A., Fotiadis, D. I. & Massalas, C. V. (2001) Elastic stability of silicone ferrofluid internal tamponade (SFIT) in retinal detachment surgery. *J. Magn. Magn. Mater.*, **225**, 248–255.

Weber, H. & Landwehr, G. (1982). A new method for the determination of the mechanical properties of the vitreous. *Ophthalmic Res.*, **14**, 326–334.

Weber, H., Landwehr, G., Klip, H. & Neubauer, H. (1982) The mechanical properties of the vitreous of pig and human donor eyes. *Ophthalmic Res.*, **14**, 335–343.

Wilkinson, R. P. & Rice, T. A. (1997) *Michels Retinal detachment*, 2nd edn. St. Louis: Mosby.

Wollensak, G. & Spoerl, E. (2004) Collagen crosslinking of human and porcine sclera. *J. Cataract Refract. Surg.*, **3**, 689–695.

Woo, S. L., Kobayashi, A. S., Lawrence, C. & Schlegel, W. A. (1972a) Mathematical model of the corneal scleral shell as applied to intraocular pressure–volume relations and applanation tonometry. *Ann. Biomed. Eng.*, **1**, 87–98.

Woo, S. L., Kobayashi, A. S., Schlegel, W. A. & Lawrence, C. (1972b) Nonlinear material properties of intact cornea and sclera. *Exp. Eye Res.*, **1**, 29–39.

Wu, W., Peters, W. H. III & Hammer, M. E. (1987) Basic mechanical properties of retina in simple elongation. *ASME J. Biomed. Eng.*, **109**, 65–67.

Appendix. Constitutive relations and deformation measures

The constitutive relations, strain-displacement and curvature-displacement relations for the shell theory employed in this work (see, for example, Timoshenko & Woinowsky-Krieger, 1959) are given below.

$$N_{\varphi\varphi}^{(j)} = C[\varepsilon_{\varphi\varphi}^{(j)}(\varphi) + \nu\, \varepsilon_{\theta\theta}^{(j)}(\varphi)], \quad N_{\theta\theta}^{(j)} = C[\varepsilon_{\theta\theta}^{(j)}(\varphi) + \nu\, \varepsilon_{\varphi\varphi}^{(j)}(\varphi)], \tag{A.1}$$

$$M_{\varphi\varphi}^{(j)} = D[\chi_{\varphi\varphi}^{(j)}(\varphi) + \nu\, \chi_{\theta\theta}^{(j)}(\varphi)], \quad M_{\theta\theta}^{(j)} = D[\chi_{\theta\theta}^{(j)}(\varphi) + \nu\, \chi_{\varphi\varphi}^{(j)}(\varphi)], \tag{A.2}$$

$$\varepsilon_{\varphi\varphi}^{(j)}(\varphi) = \frac{1}{R}\{u_j'(\varphi) - w_j(\varphi)\}, \quad \varepsilon_{\theta\theta}^{(j)}(\varphi) = \frac{\cot\varphi}{R}\{u_j(\varphi) - w_j(\varphi)\tan\varphi\}, \tag{A.3}$$

$$\chi_{\varphi\varphi}^{(j)}(\varphi) = \frac{1}{R^2}\{u_j'(\varphi) + w_j''(\varphi)\}, \quad \chi_{\theta\theta}^{(j)}(\varphi) = \frac{\cot\varphi}{R^2}\{u_j(\varphi) + w_j'(\varphi)\}. \tag{A.4}$$